# A Novel Multilevel Solid-State Transformer for Hybrid Power Grids


Vitor Monteiro
*Centro ALGORITMI*
*University of Minho*
Guimaraes, Portugal
vmonteiro@dei.uminho.pt

Delfim Pedrosa
*Centro ALGORITMI*
*University of Minho*
Guimaraes, Portugal
dpedrosa@dei.uminho.pt

Sergio Coelho
*Centro ALGORITMI*
*University of Minho*
Guimaraes, Portugal
sergio.coelho@algoritmi.uminho.pt

Tiago Sousa
*Centro ALGORITMI*
*University of Minho*
Guimaraes, Portugal
tsousa@dei.uminho.pt

Luis Machado
*Centro ALGORITMI*
*University of Minho*
Guimaraes, Portugal
lmachado@dei.uminho.pt

Joao L. Afonso
*Centro ALGORITMI*
*University of Minho*
Guimaraes, Portugal
jla@dei.uminho.pt



***Abstract*—This paper presents a new proposed topology of a solid-state transformer (SST) for application in hybrid power grids (ac and dc), in which the possibility of operating with various voltage levels (multilevel) in both sides is the main characteristic. At the interface with the power grid (primary side), the proposed SST consists of an ac-dc converter in Y configuration that guarantees operation with five levels in each phase-to-neutral voltage. To establish the hybrid power grid on the secondary side, the SST is composed of a dc-ac converter in Y configuration to establish an ac-grid, also operating with five levels in each phase-to-neutral voltage, and by a dc-dc converter to establish a dc-grid, which operates with three voltage levels. The interface between the converters of the primary side and the secondary side is guaranteed by an intermediary isolated dc-dc converter. As fundamental requirements, the proposed SST operates with balanced and sinusoidal currents on the primary side, and with balanced and sinusoidal voltages on the secondary side (ac-grid), as well as controlled voltages and currents on the dc-grid. Throughout the paper, the proposed topology for the SST is described in detail, with the operating principle of each converter being presented. The obtained results, both on steady-state and transient-state, for several main operating conditions, prove the correct functioning of the proposed SST, highlighting important features that contextualize the operation of the proposed SST in smart grids.**



***Keywords—Solid-State Transformer, Hybrid Power Grids, Smart Grids.***


## I. INTRODUCTION

As predominantly revealed mainly along the last decade, the applicability of solid-state transformers (SSTs) toward diverse purposes in smart grids is seen as an emergent technology as a compromise to replace traditional transformers, offering a set of advantages based on the improved power controllability and power quality in both sides, i.e., power grid and loads [1][2]. The preview applicability of the SST as a key component in the actual and imminent distribution grids is presented in [3], highlighting technical concerns and potential restrictive issues. A broad summary regarding the origins and progress of main conceptions of SSTs is accessible in [4] and the investigation of the SST abilities for a smart and resilient grid is debated in [5]. The SST permits the assimilation of vital technologies as is the case of renewables, electric mobility, and storage systems, also offering a rapid regulation according to the loads operation [6][7][8]. A review regarding the state-of-the-art of SSTs focusing on key features as related to improved power electronics topologies, concerns of practical implementation, and up-to-date progress and challenges is introduced in [9]. Considering the relevance of the SST for smart grids, the scope of applications is increasingly broadened. In this circumstance, an energy management plan by means of SSTs is discussed in [10], an SST interfacing dispersed renewables based on photovoltaic is presented in [11], the perspective of using SSTs for renewables based on wind power systems is presented in [12], a new control algorithm aiming the efficiency optimization of a dc SST for interface renewables based on photovoltaics in presented in [13], the modeling and design of an SST for microgrid applications is studied in [14], and the applicability of the SST for distribution systems, concerning a review of technologies, sustained functionalities, and construction aspects, is presented in [15], while concerning the applications of SST, the expansion challenges, and future perspectives to incorporate the SST in distribution systems is presented in [16]. In terms of internal constitution, to guarantee the ac interfaces in both primary-side and secondary-side, an SST is composed by a set of power electronics converters, imposing buck or boost features, which likewise occurs with a conventional low-frequency transformer, but with the galvanic isolation assured by a high-frequency transformer. Furthermore, when compared with the conventional low-frequency transformer, an SST has the possibility to reduce the volume and weight for the same nominal power, also indicating an attractive achievement for numerous applications in smart grids. A couple of illustrative cases are offered in [17], [18], and [19].

The main features of an SST over a conventional transformer are related to the instantaneous output voltage regulation for all conditions of the power grid voltage and related to the operation with unitary power factor for the ac power grid side, independently of the power quality problems caused by the loads. The possibility of controlling an SST to operate with some of these characteristics is explored in [20] and [21]. Supported by the aforementioned features, this paper presents as pertinent contributions: (a) A novel structure based on bidirectional multilevel power converters in both sides of the SST; (b) Application of the proposed SST for hybrid power grids (an ac-grid and a dc-grid on the secondary-side); (c) Comprehensive demonstration of new operation


978-1-7281-7660-4/21/$31.00 ©2021 IEEE

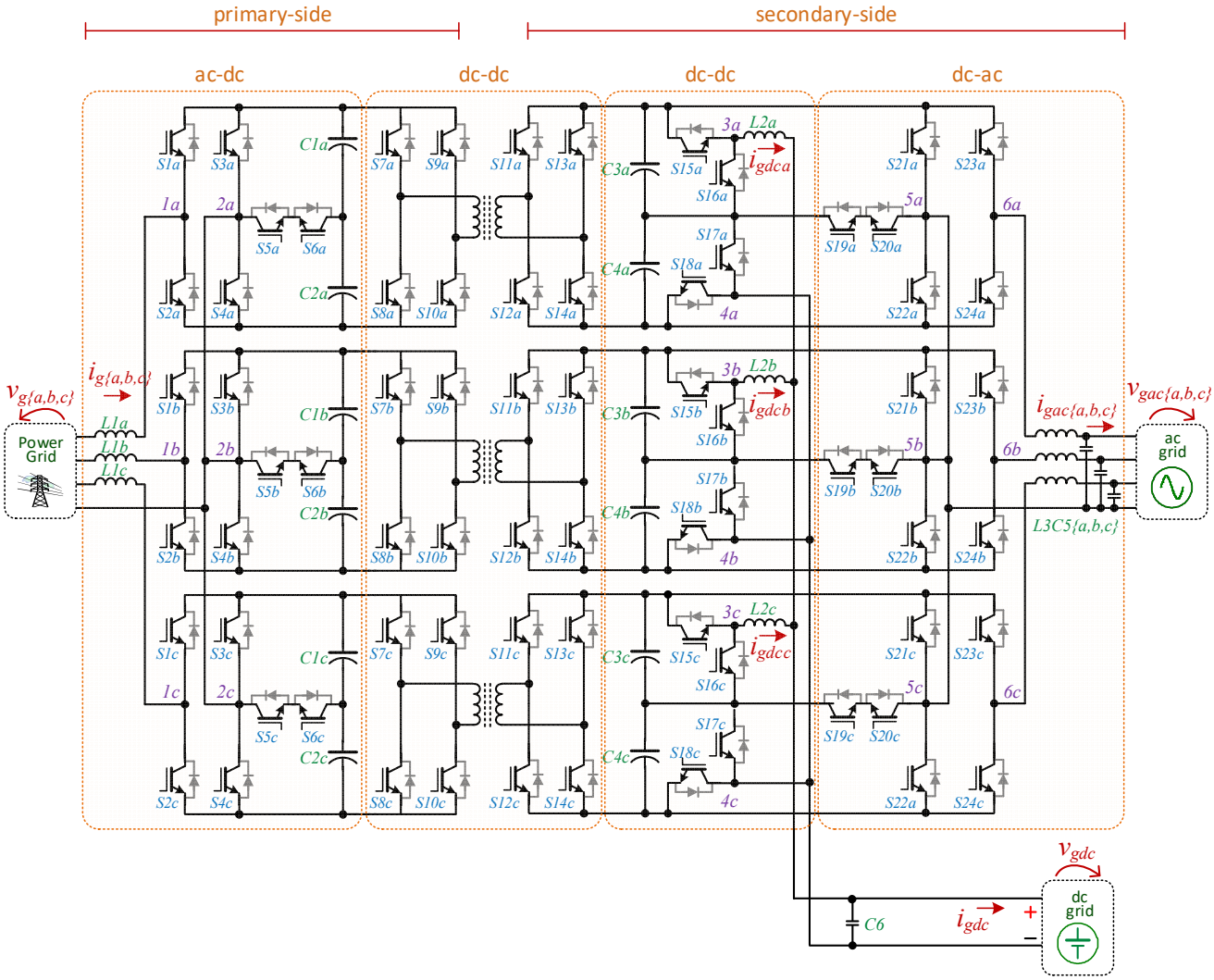



Fig. 1. Power electronics structure of the proposed multilevel solid-state transformer (SST) for hybrid power grids.

opportunities of the SST framed in smart grids; (d) Computational validation considering realistic conditions of operation in terms of power quality issues for the power grid voltage and for the load-side current. The addressed topic is aligned with the SST architectures in the literature, where the main contribution is related with the topologies, i.e., the paper gives an innovative answer as alternative to the traditional full-bridge converters used in SST.

## II. Multilevel Solid-State Transformer: Description of the Power Electronics Structure

Globally, the structure of the proposed multilevel SST is based on four main blocks: an ac-dc converter; an isolated dc-dc converter; a dc-ac converter to interface the ac-grid, where are connected the ac loads; a dc-dc converter to interface the dc-grid, where are connected the dc loads. The complete structure of the SST is presented in Fig. 1. As shown, the ac-dc converter used to interface the power grid is constituted by a bidirectional multilevel arrangement that permits to operate with five voltage levels in each phase-to-neutral, where each phase is individually controlled, offering more flexibility in terms of controllability. Moreover, since each phase can be individually controlled, it offers more interesting solutions in terms of redundancy. One of the advantages of the proposed SST is the fact that the IGBTs $S_{1\{a,b,c\}}$ and $S_{2\{a,b,c\}}$ are switched at the fundamental frequency of the power grid voltage. As shown, this block is formed by 18 switching devices, where 2 switching devices in each phase are used to form a bidirectional and bipolar element, fundamental to obtain the intermediary voltage levels of $+v_{dc}/2$ and $-v_{dc}/2$ using the split dc-link. Since the ac-dc converter has a Y configuration, the neutral point is connected to each bidirectional and bipolar cell presented in each phase. As coupling filters for the ac power grid side were considered inductors ($L$) to simplify the analysis, however, other types can be considered (e.g., $LC$ or $LCL$), but such analysis is out of the scope of this paper. Regarding the block that corresponds to the isolated dc-dc converter, dual-active bridge converters were considered, each one for each phase (i.e., each phase of the dc-dc is linked to each phase of the ac-dc). This intermediary block is responsible to guarantee the necessary galvanic isolation and, since it is used to interface the ac-dc and the dc-ac blocks, a conventional solution was considered. As shown, this block is formed by 24 switching devices and by three high-frequency transformers. The dc-ac block is linked to the isolated dc-dc, where the respective phases are linked together. The dc-ac converter is also constituted by a bidirectional multilevel structure, permitting to operate with five voltages levels. This is a very interesting feature since the dc-ac converter is responsible to control the voltages applied to the loads (i.e., each phase-to-neutral voltage), and different types of loads can be connected (e.g., unbalanced loads and

individual transient-state in the phases). Also in this converter, one of the advantages is the fact that the IGBTs $S_{23\{a,b,c\}}$ and $S_{24\{a,b,c\}}$ are switched at the frequency of the power grid voltage. As shown, the dc-ac block is also formed by 18 switching devices, in the same way as the ac-dc block. In this case, as coupling filters were considered *LC* filters for each phase. The dc-ac converter also has a Y configuration, where the neutral point is connected to each bidirectional and bipolar cell presented in each phase. The dc-dc converter on the secondary-side also operates with a multilevel feature, in this case permitting to operate with three voltage levels according to the output voltages of the block formed by the isolated dc-dc. This dc-dc block is used to control the voltage and current for the dc-grid, which is part of the hybrid power grid. As shown, this block is formed by 12 switching devices and a *L* filter is considered in each phase, where the distinct outputs are connected in parallel. In terms of scalability, the proposed architecture in terms of the individual converters can be used, e.g., for modular multilevel structures, both at the primary and secondary side.

## III. Multilevel Solid-State Transformer: Control Algorithms

This section introduces the principle of operation of the control algorithms used to control each converter of the SST. Regarding the ac-dc converter used to interface the power grid, the references for the power grid currents are determined using the Fryze-Buchholz-Depenbrock theory, permitting to obtain three reference currents ($i_{g\{a,b,c\}}$*) proportional to the power grid voltages ($v_{g\{a,b,c\}}$) and the operating power of the SST [22][23][24]. In this perspective, it can be established:

$$i_{g\{a,b,c\}}{}^{*} = \frac{v_{g\{a,b,c\}}}{V_{G\{a,b,c\}}{}^{2}}\, P_G\,, \tag{1}$$

where $P_G$ corresponds to the operating active power of the SST and the power necessary to control the dc-link voltage. The waveform of the reference current is obtained using a phase-locked loop (PLL). The dc-link voltages are controlled by PI controllers. To control the power grid currents, a predictive strategy is considered. Based on the analysis of voltages and current on the ac power grid side, it can be proven that:

$$v_{\{a,b,c\}}{}^{*} = \frac{v_{g\{a,b,c\}}}{v_{dc}} - L_{\{a,b,c\}}\frac{di_{g\{a,b,c\}}}{dt}, \tag{2}$$

where the digital implementation results in:

$$i_{g\{a,b,c\}}[k+1] = \left(v_{g\{a,b,c\}}[k] - \frac{v_{\{a,b,c\}}{}^{*}[k]}{v_{dc}[k]}\right)\frac{T_s}{L_{\{a,b,c\}}} + i_{g\{a,b,c\}}[k]\,, \tag{3}$$

where $i_{g\{a,b,c\}}[k+1]$ is the reference that the current $i_{g\{a,b,c\}}[k]$ must reach, and the voltage $v_{\{a,b,c\}}$*$[k+1]$ is the voltage that the converter must produce to obtain the desired current. Since in the scope of this paper it is considered a strategy to guarantee the operation with fixed switching frequency, therefore, the voltage $v_{\{a,b,c\}}$*$[k]$ is compared with a PWM carrier, during each sampling period, to define the state of the converter.

Regarding the isolated dc-dc converter, in the scope of this paper it was considered a phase-shift strategy. Regarding the control of the dc-ac converter, it should be noted that this converter must be controlled with voltage feedback, which is quite different from the control established for the ac-dc converter on the primary-side. The voltage control aims the production of balanced and sinusoidal voltages with nominal values of rms and frequency. By analyzing the voltage and currents, it is possible to establish:

$$v_{\{a,b,c\}}{}^{*} = L_{3\{a,b,c\}}C_{5\{a,b,c\}}\frac{d^2v_{gac\{a,b,c\}}}{dt^2} - L_{3\{a,b,c\}}\frac{di_{gac\{a,b,c\}}}{dt} + v_{gac\{a,b,c\}}\,, \tag{4}$$

where, by considering differential equations to estimate the linear variations, the final digital control equation is established as:

$$v_{\{a,b,c\}}{}^{*} = \frac{L_{3\{a,b,c\}}C_{5\{a,b,c\}}}{T_a{}^{2}}\left(v_{gac\{a,b,c\}}{}^{*}[k] - 2v_{gac\{a,b,c\}}[k] + v_{gac\{a,b,c\}}[k-1]\right) + v_{gac\{a,b,c\}}[k] - \frac{L_1}{T_a}\left(i_{gac\{a,b,c\}}[k] - i_{gac\{a,b,c\}}[k-1]\right), \tag{5}$$

where $v_{gac\{a,b,c\}}$*$[k]$ is the reference voltage for the converter and the voltage $v_{\{a,b,c\}}$*$[k]$ is the voltage that the converter must produce (between the points $5\{a,b,c\}$ and $6\{a,b,c\}$, as shown in Fig. 1) in order to obtain the desired voltage, which is compared with a PWM carrier.

Regarding the dc-dc converter on the secondary-side (dc-grid), it can be controlled with voltage or current feedback. Moreover, since it can operate in bidirectional mode, it should be controlled in buck-mode (when the dc-grid is delivering energy) or in boost-mode (when the dc-grid is receiving energy). During the operation in buck-mode, by controlling the duty-cycle it is possible to control the converter with voltage feedback. On the other hand, for controlling with current feedback during the operation in buck-mode, by analyzing the voltages and currents, it can be established:

$$v_{\{a,b,c\}}{}^{*} = v_{gdc} + L_{2\{a,b,c\}}\frac{di_{gdc\{a,b,c\}}}{dt}, \tag{6}$$

where the digital implementation results in

$$i_{gdc\{a,b,c\}}[k+1] = \left(v_{\{a,b,c\}}{}^{*}[k] - v_{gdc}[k]\right)\frac{T_s}{L_{2\{a,b,c\}}} + i_{gdc\{a,b,c\}}[k], \tag{7}$$

where the current $i_{gdc}[k+1]$ is the current that must be reached by the current $i_{gdc}[k]$, and $v_{\{a,b,c\}}$* is the voltage that the converter must produce (between the points $3\{a,b,c\}$ and $4\{a,b,c\}$, as shown in Fig. 1) and, consequently, being compared with the PWM carrier to define the state of the converter. On the other hand, when it is necessary to control the current in boost-mode, also by analyzing the voltages and currents, it can be established:

$$v_{\{a,b,c\}}{}^{*} = v_{gdc} - L_{2\{a,b,c\}}\frac{di_{gdc\{a,b,c\}}}{dt}, \tag{8}$$

where the digital implementation results in

$$i_{gdc\{a,b,c\}}[k+1] = \left(v_{gdc}[k] - v_{\{a,b,c\}}{}^{*}[k]\right)\frac{T_s}{L_{2\{a,b,c\}}} + i_{gdc\{a,b,c\}}[k], \tag{9}$$

where the current $i_{gdc}[k+1]$ is the current that must be reached by the current $i_{gdc}[k]$, and $v_{\{a,b,c\}}$* is the voltage that the converter must produce (between the points $3\{a,b,c\}$ and $4\{a,b,c\}$, as shown in Fig. 1) and, therefore, being compared with the PWM carrier to define the state of the converter.

## IV. Solid-State Transformer: Validation

The validation was performed with the PSIM software considering a phase-to-phase voltage on the ac power grid side of 400 V, a phase-to-phase voltage on the ac-side of 400 V (secondary-side), a dc-link voltage of 800 V in both sides, an

$L$ filter on the ac power grid side of 5 mH, an $LC$ filter on the ac-grid of 5 mH and 1 µF, a sampling frequency of 40 kHz, and a switching frequency of 20 kHz. The obtained results are satisfactory and corroborate the characteristics listed as added value of the proposed SST, however, it is important to note that other nominal values could have been considered, either for the values of voltages and operating powers, and in no way it would change the operation of the SST. The values considered are examples of a specific case of application. The same is true for the values of the passive components.

Fig. 2 shows the three phase-to-neutral power grid voltages ($v_{ga}$, $v_{gb}$, $v_{gc}$), where it can be seen that they are not purely sinusoidal (THD of 3.6%), as well as the three currents ($i_{ga}$, $i_{gb}$, $i_{gc}$). This result is of particular importance because it highlights one of the most valuable assets of SST, in which the currents on the ac power grid side are almost purely sinusoidal (with a THD of 0.7%) despite the distortion of the voltages. In addition to being purely sinusoidal, the currents are in phase with the respective voltages. It is also possible to see that the currents are properly balanced, despite the slight imbalance of voltages.

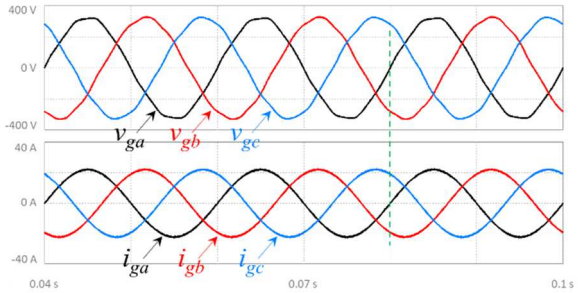



Fig. 2. SST operation, regarding the ac-dc converter, with sinusoidal grid currents and unitary power factor: Power grid voltages ($v_{ga}$, $v_{gb}$, $v_{gc}$); Power grid currents ($i_{ga}$, $i_{gb}$, $i_{gc}$).

Fig. 3 shows, once again, the voltages ($v_{ga}$, $v_{gb}$, $v_{gc}$) and currents ($i_{ga}$, $i_{gb}$, $i_{gc}$) in a case where the currents present a sinusoidal waveform, are properly balanced, but have a slight lag of 20º in relation to the respective voltages. This result was obtained to illustrate one of the potentials of the SST in the perspective of contributing to the improvement of the power quality on the ac power grid side. In terms of operation with active power, this result is the same as the previous case ($P$ = 10.8 kW), but it also operates with reactive power ($Q$ = 3.5 kVAr). In addition to the active power necessary for its correct functioning (i.e., according to the loads or sources on the secondary side) the SST can also operate with reactive power. This result only makes sense in a perspective of operation in smart grids, in which the value of the reactive power is defined by the smart grid and transmitted to the SST. The value of reactive power is an input to the control algorithm that helps to define the reference currents; however, this analysis is out of the scope of this paper. Following the same logic as in the previous case, Fig. 4 shows the voltages ($v_{ga}$, $v_{gb}$, $v_{gc}$) and currents ($i_{ga}$, $i_{gb}$, $i_{gc}$) in a case where the SST allows the operation with current harmonics. Thus, in addition to the operation with the rated power ($P$ = 10.8 kW), each phase operates with a third-order current harmonic (with a rms current value of 10 A). Once again, it is important to note that this result only makes sense in a context of smart grid operation, improving the power quality and not affecting the rest of the SST operation. By analyzing one of the main advantages of the proposed SST, Fig. 5 shows the three phase-to-neutral voltages ($v_{ga}$, $v_{gb}$, $v_{gc}$) and the operating voltages in each phase ($v_{aba1}$, $v_{abb1}$, $v_{abc1}$), measured between the points 1{*a,b,c*} and 2{*a,b,c*}, as indicated in Fig. 1. The spikes are due to the PWM, but without causing any disturbance in the SST operation. In each phase, the SST operates with five different voltage levels. As it is possible to verify, the time in which each ac-dc converter assumes a certain voltage level is not the same for all voltage levels (i.e., it is perfectly visible that the time that the converter stays between levels 0 and $v_{dc}$/2 is considerably less than the time in which the converter operates between the levels $v_{dc}$/2 and $v_{dc}$), because this is the only way to obtain sinusoidal currents. This result corroborates the multilevel characteristic of the proposed SST.

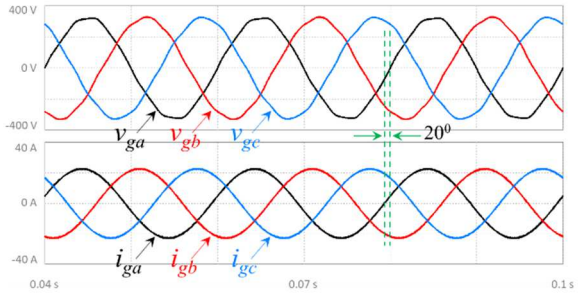



Fig. 3. SST operation, regarding the ac-dc converter, with sinusoidal grid currents and producing reactive power: Power grid voltages ($v_{ga}$, $v_{gb}$, $v_{gc}$); Power grid currents ($i_{ga}$, $i_{gb}$, $i_{gc}$).

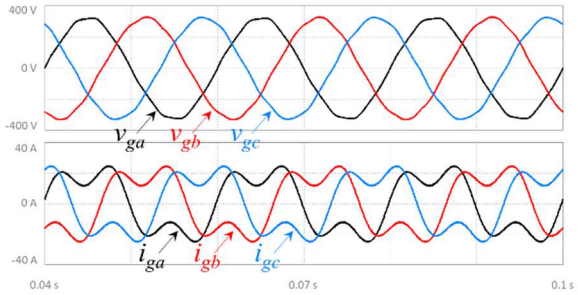



Fig. 4. SST operation, regarding the ac-dc converter, with non-sinusoidal grid currents: Power grid voltages ($v_{ga}$, $v_{gb}$, $v_{gc}$); Power grid currents ($i_{ga}$, $i_{gb}$, $i_{gc}$).

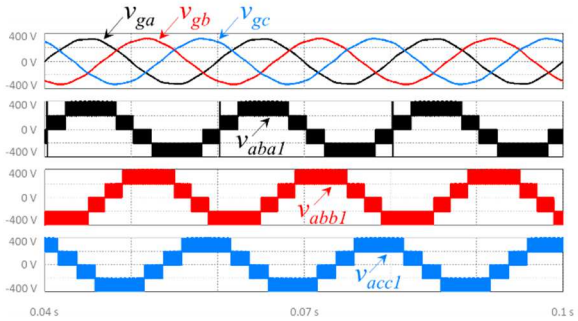



Fig. 5. SST operation regarding the operating voltages of the ac-dc converter: Power grid voltages ($v_{ga}$, $v_{gb}$, $v_{gc}$); Operating voltages ($v_{aba1}$, $v_{abb1}$, $v_{acc1}$).

Fig. 6 shows (for phase $a$) the modulation strategy. To obtain the five voltage levels, a modified sinusoid is compared with the PWM carrier ($c_{pwm}$). As previously highlighted, one of the advantages of the proposed SST is the fact that the IGBTs $S_1$ and $S_2$ are switched at the frequency of the power grid voltage: when the voltage is positive, the IGBT $S_1$ is on and the IGBT $S_2$ is off; when the voltage is negative, the $S_1$ is

off and $S_2$ is on. The comparison of the $a_{pwm}$ signal with the PWM carrier ($c_{pwm}$) allows to obtain the control signals for the IGBT $S_3$, however, on the other hand, the comparison of the $b_{pwm}$ signal with the PWM carrier ($c_{pwm}$) allows to obtain the control signals for the IGBT $S_4$. As shown, the IGBTs $S_3$ and $S_4$ are not always switched over a period of the voltage: the IGBT $S_4$ is mainly switched when the voltage is positive and the IGBT $S_3$ when the voltage is negative. On the other hand, the IGBTs $S_5$ and $S_6$ (considered as a single switching device) always switch over a period of the power grid voltage. Regarding the secondary-side, Fig. 7 shows the voltages produced by the SST ($v_{gaca}$, $v_{gacb}$, $v_{gacc}$) and the consumed currents by the loads ($i_{gaca}$, $i_{gacb}$, $i_{gacc}$). The SST produces three sinusoidal and properly balanced voltages (400 V - 50 Hz), regardless of the currents consumed (non-linear loads were considered, presenting a THD of 13%). This result validates one of the fundamental characteristics of the SST, which consists of producing three sinusoidal (THD of 1%) and balanced voltages, regardless of the loads. The dc-ac converter also operates with multilevel characteristics in each phase.

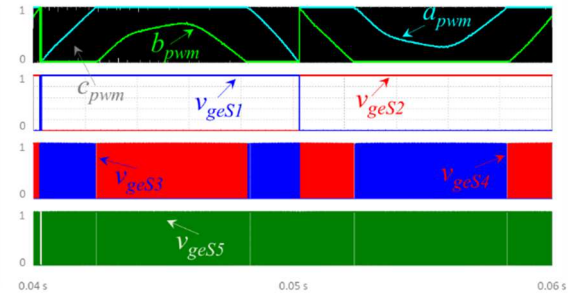



Fig. 6. SST operation regarding the PWM strategy of the ac-dc converter: PWM carrier ($c_{pwm}$); Control signals ($a_{pwm}$, $b_{pwm}$); Gate-emitter voltage of the IGBTs ($v_{geS1}$, $v_{geS2}$, $v_{geS3}$, $v_{geS4}$, $v_{geS5}$).

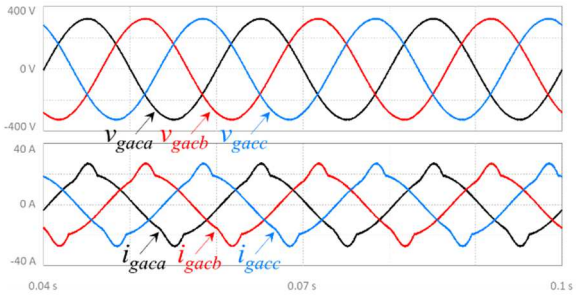



Fig. 7. SST operation, regarding the dc-ac converter, with sinusoidal load voltages: Voltages on the ac-grid ($v_{gaca}$, $v_{gacb}$, $v_{gacc}$); Currents on the ac-grid ($i_{gaca}$, $i_{gacb}$, $i_{gacc}$).

Fig. 8 shows the voltages ($v_{gaca}$, $v_{gacb}$, $v_{gacc}$) produced by the SST and the operating five voltages levels in each phase ($v_{aba2}$, $v_{abb2}$, $v_{abc2}$), measured between the points 5{*a,b,c*} and 6{*a,b,c*}. Regarding the multilevel dc-dc converter on the secondary-side, Fig. 9 shows the voltage on the dc-grid ($v_{gdc}$), the current consumed by the loads ($i_{gdc}$), and the operating voltages of the converter ($v_{abdc1}$, $v_{abdc2}$, $v_{abdc3}$). In this specific case, a voltage of 150 V was simulated for the dc-grid and an operating power of 4.5 kW was considered. Since the voltage of the dc-grid is lower than half of the dc-link voltage in each phase of the dc-dc converter, each voltage ($v_{abdc1}$, $v_{abdc2}$, $v_{abdc3}$) varies between 0 and $v_{dc}/2$. Like to the case shown in Fig. 9, the same variables are shown in Fig. 10, but with the converter producing a voltage of 250 V for the dc-grid. In addition, in this situation, the operating power has increased to 7.5 kW. In this specific case, as the voltage imposed on the dc-grid is greater than half of the dc-link voltage, each voltage ($v_{abdc1}$, $v_{abdc2}$, $v_{abdc3}$) varies between $v_{dc}/2$ and $v_{dc}$. Based on such results, it is verified that the operation with three different voltage levels (0, $v_{dc}/2$, $v_{dc}$) is significantly relevant in comparison with the traditional converters (e.g., buck or boost), since it allows to reduce the maximum voltage applied to each IGBT.

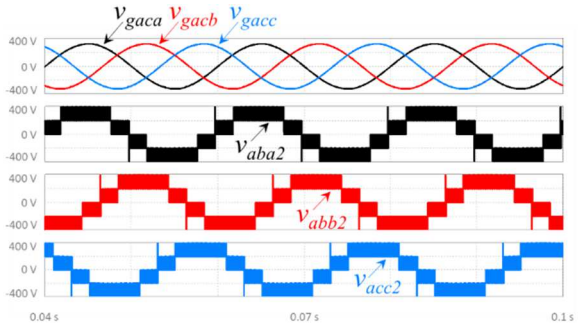



Fig. 8. SST operation regarding the operating voltages of the dc-ac converter: Voltages on the ac-grid ($v_{gaca}$, $v_{gacb}$, $v_{gacc}$); Operating voltages ($v_{aba2}$, $v_{abb2}$, $v_{acc2}$).

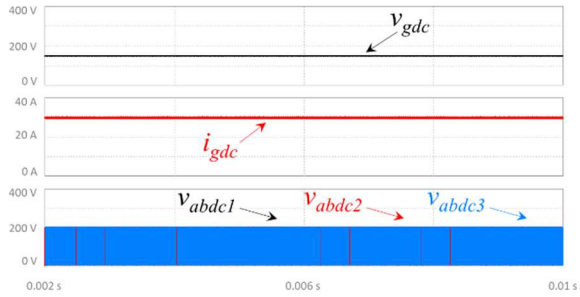



Fig. 9. SST operation regarding the dc-dc converter on the dc-grid with an output voltage higher than half of the dc-link voltage: Voltage on the dc-grid ($v_{gdc}$); Current on the dc-grid ($i_{gdc}$); Operating voltages ($v_{abdc1}$, $v_{abdc2}$, $v_{abdc3}$).

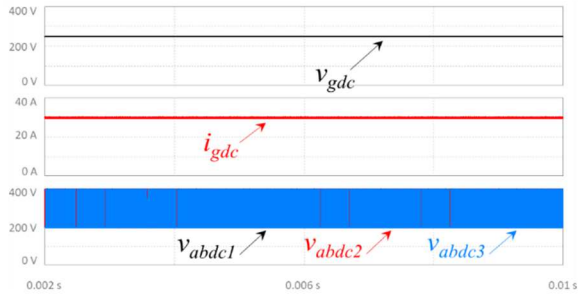



Fig. 10. SST operation regarding the dc-dc converter on the dc-grid with an output voltage lower than half of the dc-link voltage: Voltage on the dc-grid ($v_{gdc}$); Current on the dc-grid ($i_{gdc}$); Operating voltages ($v_{abdc1}$, $v_{abdc2}$, $v_{abdc3}$).

To analyze the dynamic operation of the dc-dc converter operating with the three voltage levels (0, $v_{dc}/2$, $v_{dc}$), the same variables are shown in Fig. 11, but considering a variation in the operating power. In a first case, the converter is operating with a power of 7.5 kW, and the converter operates with the voltages ranging between $v_{dc}/2$ and $v_{dc}$. When a transition in the operating power occurs (in this case, the operating power has been reduced to 3.75 kW), the converter temporarily assumes the three voltage levels. Subsequently, in a steady-state, the converter resumes the operation with the voltages varying between $v_{dc}/2$ and $v_{dc}$, regardless of the operating power. It is important to highlight that this transition

occurs until the converter operates again in a steady-state. Fig. 12 shows, in detail, the moment of the transient-state to perform a more detailed analysis. The transition takes a time interval that corresponds to two switching periods ($2T_{SW}$) and, in this interval, the operating voltages of the converter ($v_{abdc1}$, $v_{abdc2}$, $v_{abdc3}$) clearly assume the three voltage levels (0, $v_{dc}$/2, $v_{dc}$). Due to the proposed control algorithm, the current has a ripple with a frequency that is six times higher than the switching period, which allows to significantly reduce the value of the passive components.

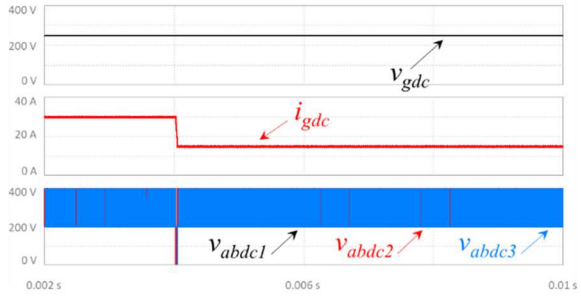



Fig. 11. SST operation regarding the dc-dc converter on the dc-grid with an output voltage higher than half of the dc-link voltage and with a transient-state in the operating power: Voltage on the dc-grid ($v_{gdc}$); Current on the dc-grid ($i_{gdc}$); Operating voltage ($v_{abdc1}$, $v_{abdc2}$, $v_{abdc3}$).

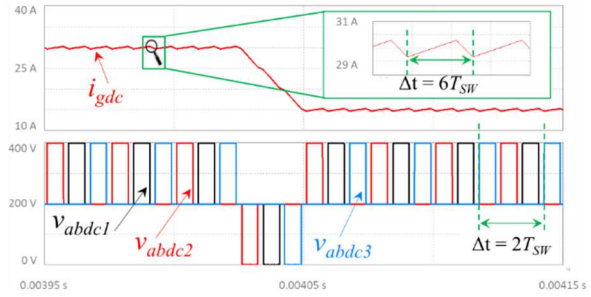



Fig. 12. SST operation regarding the dc-dc converter on the dc-grid with an output voltage higher than half of the dc-link voltage and with a detail of the transient-state: Current on the dc-grid ($i_{gdc}$); Operating voltage ($v_{abdc1}$, $v_{abdc2}$, $v_{abdc3}$).

## V. Conclusions

This paper presents a new proposed topology of a solid-state transformer (SST) for hybrid power grids, in which the possibility of operating with different voltage levels (multilevel) is the main characteristic, both for the primary-side and the secondary-side. Throughout the paper, the proposed SST is described in detail, with the principle of operation being properly presented, as well as the digital control equations and the fundamental aspects of the modulation to guarantee the voltage levels. The obtained results, both on a steady-state and transient-state, prove the correct functioning of the SST, showing important features for contextualizing the SST operation in smart grids, namely the possibility of operating with reactive power and/or current harmonics to act with compensation characteristics to improve the power quality at the ac power grid side. The validation was obtained for the most relevant operating conditions.

## Acknowledgment

This work has been supported by FCT – Fundação para a Ciência e Tecnologia within the R&D Units Project Scope: UIDB/00319/2020. This work has been supported by the FCT Project newERA4GRIDs PTDC/EEI-EEE/30283/2017, and by the FCT Project DAIPESEV PTDC/EEI-EEE/30382/2017. Tiago Sousa is supported by the doctoral scholarship SFRH/BD/134353/2017 granted by FCT.

## References

[1] Y. Ko, A. Chub, L. Costa, M. Andresen, M. Liserre, "Smart transformer universal operation," IEEE APEC Applied Ppowerower Electronics Conference and Exposition, pp.1609-1616, San Antonio, TX, Apr. 2018.

[2] H. S. Krishnamoorthy, P. N. Enjeti, J. J. Sandoval, "Solid State Transformer for Grid Inter-face of High Power Multi-Pulse Rectifiers," IEEE Trans. Ind. Appl., vol.54, no.5, pp.5504-5511, Dec. 2017.

[3] J. E. Huber, J. W. Kolar, "Applicability of Solid-State Transformers in Today's and Future Distribution Grids," IEEE Trans. Smart Grid, vol.10, no.1, pp.317-326, Jan. 2019.

[4] J. E. Huber, J. W. Kolar, "Solid-State Transformers: On the Origins and Evolution of Key Concepts," in IEEE Industrial Electronics Magazine, vol. 10, no. 3, pp. 19-28, Sept. 2016.

[5] A. Q. Huang, "Medium-Voltage Solid-State Transformer: Technology for a Smarter and Resilient Grid," in IEEE Industrial Electronics Magazine, vol. 10, no. 3, pp. 29-42, Sept. 2016.

[6] N. Gorla, S. Kolluri, S. Panda, "Solid state transformer control aspects for various smart grid scenarios," IEEE ISGT Innovative Smart Grid Technologies – Asia, Auckland, pp.1-6, Dec. 2017.

[7] A. C. Nair, B. G. Fernandes, "A novel multi-port solid state transformer enabled isolated hybrid microgrid architecture," IEEE IECON Annual Conference of the Industrial Electronics Society, Beijing, pp.651-656, Nov. 2017.

[8] V. Satyamsetti, A. Michealides, A. Hadjiantonis, "Forecasting on solid state transformer applications," IEEE ICISS International Conference on Intelligent Sustainable Systems, pp.330-335, Palladam, Dec. 2017.

[9] M. A. Hannan et al., "State of the Art of Solid-State Transformers: Advanced Topologies, Implementation Issues, Recent Progress and Improvements," IEEE Access, vol.8, pp.19113-19132, 2020.

[10] Q. Chen, N. Liu, C. Hu, L. Wang, J. Zhang, "Autonomous Energy Management Strategy for Solid-State Transformer to Integrate PV-Assisted EV Charging Station Participating in Ancillary Service," IEEE Trans. Ind. Informat., vol.13, no.1, pp.258-269, Feb. 2017.

[11] H. Zhao, T. Zhu, et al., "Research on the smart modular cascaded solid-state transformer interfaced to distributed photovoltaic power generation system," IEEE Journal of Engineering, vol.2017, no.13, pp.1872-1879, 2017.

[12] I. Syed, V. Khadkikar, "Replacing the Grid Interface Transformer in Wind Energy Con-version System with Solid-State Transformer," IEEE Trans. Power Sys., vol.32, no.3, pp.2152-2160, May 2017.

[13] H. Shi, H. Wen, Y. Hu, Y. Yang, Y. Wang, "Efficiency Optimization of DC Solid-State Transformer for Photovoltaic Power Systems," IEEE Trans. Ind. Electron., vol.67, no.5, pp.3583-3595, May 2020.

[14] S. Madichetty, B. Duggal, A. Borgaonkar, S. Mishra, "Modeling and Design of Solid-State Smart Transformer for Microgrid," IEEE IEEMA Engineer Infinite Conference (eTechNxT), pp.1-6, June 2018.

[15] S. A. Saleh et al., "Solid-State Transformers for Distribution Systems–Part I: Technology and Construction," IEEE Trans. Ind. Appl., vol.55, no.5, pp.4524-4535, Sept.-Oct. 2019.

[16] S. A. Saleh et al., "Solid-State Transformers for Distribution Systems–Part II: Deployment Challenges," IEEE Trans. Ind. Appl., vol.55, no.6, pp.5708-5716, Nov.-Dec. 2019.

[17] H. Chen, D. Divan, "Design of a 10-kV·A Soft-Switching Solid-State Transformer (S4T)," IEEE Trans. Power Electron., vol.33, no.7, pp.5724-5738, July 2018.

[18] J. E. Huber, J. Böhler, D. Rothmund, J. W. Kolar, "Analysis and cell-level experimental verification of a 25 kW all-SiC isolated front end 6.6 kV/400 V AC-DC solid-state transformer," CPSS Trans. On Power Electronics and Applications, vol.2, no.2, pp.140-148, Aug. 2017.

[19] L. Rodriguez, V. Jones, A. Oliva, A. Escobar-Mejía, J. Balda, "A New SST Topology Comprising Boost Three-Level AC/DC Converters for Applications in Electric Power Distribution Systems," IEEE J. Emerg. Sel. Topics Power Electron., vol.5, no.2, pp.735-746, June 2017.

[20] L. Costa, G. Carne, G. Buticchi, M. Liserre, "The Smart Transformer: A solid-state transformer tailored to provide ancillary services to the distribution grid," IEEE Power Electronics Magazine, vol.4, no.2, pp.56-67, June 2017.

[21] M. Kang, P. N. Enjeti, I. J. Pitel, "Analysis and design of electronic transformers for electric power distribution system," IEEE Trans. Power Electron., vol.14, no.6, pp.1133–1141, Nov. 1999.

[22] F. Blaabjerg, R. Teodorescu, M. Liserre, A. V. Timbus, "Overview of Control and Grid Synchronization for Distributed Power Generation Systems," IEEE Trans. Ind. Electron., vol.53, no.5, pp.1398-1409, Oct. 2006.

[23] A. Valdez-Fernández, P. Martínez-Rodríguez, et al., "A Model-Based Controller for the Cascade H-Bridge Multilevel Converter Used as a Shunt Active Filter," IEEE Trans. Ind. Electron., vol.60, no.11, pp.5019-5028, Nov. 2013.

[24] M. Depenbrock, "The FBD-Method, a Generally Applicable Tool for Analyzing Power Relations," IEEE Trans. Power Syst., vol.8, no.2, pp.381-387, May 1993.